Journal of Materials Science: Materials in Electronics (2020) 31:7193–7199
https://doi.org/10.1007/s10854-020-03291-0

One-step spray of Cu_2NiSnS_4 thin films as absorber materials for photovoltaic applications

S. Dridi[1,2] · N. Bitri[1] · S. Mahjoubi[1] · F. Chaabouni[1] · I. Ly[3]

Received: 8 February 2020 / Accepted: 20 March 2020 / Published online: 4 April 2020

Abstract
A simple one-step «Spray Pyrolysis» technique was developed for preparing Cu_2NiSnS_4 (CNTS) thin film followed by an annealing treatment process. Originally, the spray technique was successfully used to deposit the thin film onto glass substrate at 250 °C for 60 min spray duration. Again, the deposited thin film was annealed in a sulfur atmosphere at a temperature of 500 °C during 30 min. The sulfured thin film exhibits (111), (220) and (311) orientations correspond well to the cubic CNTS structure and other impurity compounds. The SEM data exhibit a uniform, rough and compact topography of CNTS thin films with an average-thickness of 1.36 µm. The absorption coefficient is found to be higher than 10^4 cm^{-1} in the visible region while the direct band energy of 1.62 eV, which is eminently suitable for use as an absorber in the solar cell. The complex impedance diagrams indicate the decrease of resistance by increasing temperature, which attributes to a semiconductor behavior. The close values of activation energies 0.63 and 0.54 eV determined from both angular frequency and DC conductivity indicate that the carrier transport mechanism is thermally activated.

1 Introduction

Copper–nickel–tin–sulfur (Cu_2NiSnS_4), one of the quaternary semiconductor materials, has been the focus of attention in recent years since its constituent elements are inexpensive, environmentally benign and widely existing in nature. Other important advantages, the CNTS material with p-type conductivity [1] has a high optical absorption coefficient [10^4–10^5 cm^{-1}] in the visible region and suitable direct optical band gap in the range of 1.1–1.5 eV [2]. These excellent properties enable to CNTS material to be used as an absorber in low-cost solar cells. In the literature, CNTS materials have been synthesized by several methods such as electrodeposition [3, 4], solvothermal [5–7], hydrothermal [1], hot injection [2], electrospinning [8], spin coating [9] and spray pyrolysis [10, 11]. This study focused on describing the chemical spray pyrolysis technique.

Generally speaking, the spray pyrolysis method for thin film deposition involves spraying a precursor solution simultaneously or sequentially [12]. For example, in our previous works [10, 11], we studied the structural, morphological, optical and electrical properties of CNTS thin films prepared by spray sandwich without any annealing treatment. This method «spray sandwich» consists of spraying the precursor solutions sequentially from NiS, SnS_2, and Cu_2S onto glass substrates at high temperatures. In the present work, we have investigated the effect of sulfurization on structural, morphological, optical and electrical properties of CNTS thin films prepared by a single step of spray. As is implied by the name, this method is based on spraying the precursor solutions simultaneously on heated glass substrates.

2 Experimental details

2.1 Synthesis of CNTS thin films

CNTS thin films were prepared by two different growth techniques: a spray process and an annealing treatment process. These two processes are described in the following.

✉ S. Dridi
dridisarra13@gmail.com

[1] Laboratoire de Photovoltaïque Et matériaux Semi-Conducteurs, Université de Tunis El Manar, Ecole Nationale D'Ingénieurs de Tunis, 1002 Tunis, Tunisia

[2] Université de Tunis, Ecole Nationale Supérieure D'Ingénieurs de Tunis, Tunis, Tunisia

[3] Centre de Recherche Paul Pascal, Université Bordeaux 1, Bordeaux, France

For the spray process, the CNTS precursors were prepared by dissolving the following constituents: 0.02 M $Ni(NO_3)_2{\cdot}6H_2O$, 0.02 M SnO_2, 0.02 M $CuSO_4$ and 0.02 M $Na_2S_2O_3{\cdot}5H_2O$ in 100 mL distilled water. The main deposition parameters of the spraying system such as the substrate temperature, the spray duration, the spray deposition rate, the gas flow rate, the distance nozzle-substrate and the hot plate rotation speed were set at: 250 °C, 60 min, 2 mL/min, 10 L/min, 20 cm, and 14 rpm, respectively. Figure 1 presents the usual equipment of spray pyrolysis.

For the annealing treatment process, the samples were sulfurized in a tube furnace under nitrogen flow at a temperatures of 450 and 500 °C for 30 min. During the heating process, the sulfur powder (0.035 g) was transformed into vapor and diffused into the layer to ensure the full-sulfurization of precursors using a nitrogen flow (1.5 L/min) which was used to prevent the oxidation of the CNTS thin films. This process is schematically presented in Fig. 2.

2.2 Characterization of CNTS thin films

X-ray diffraction (Philips X'Pert diffractometer) was used to analyze the crystalline structures of the CNTS thin films using Cu-Kα radiation ($\lambda = 1.5418$ Å) operated in the scanning angle 2θ from 10° to 70°. Further information, the operation voltage, and current were 40 kV and 30 mA, respectively. Using electron microscopy (Hitachi S-4800), the surface morphology of the CNTS thin films was investigated. UV–Vis spectrophotometer (type Shimadzu UV 3100S) was applied to ascertain the transmittance and reflectance measurements for determining the optical parameters such as the absorption coefficient and the band gap energy.

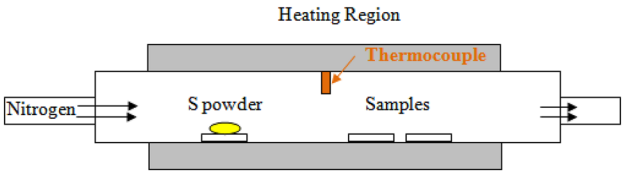

Fig. 2 Schematic diagram of the sulfurization furnace

Impedance spectroscopy was carried to measure the real and imaginary components of impedance parameters (Z' and Z'') over a wide range of temperature (713–773 °K) with a frequency of (1–13,000 kHz) through Hewlett-Packard 4192 analyzer. The results of measurements of the electrical properties of CNTS thin films give information concerning other electrical parameters, namely the conductivity σ_T, the resistance R, the frequency ω_m, and the activation energy E_a. For electrical measurements, the contact was performed using two electrodes, which were painted on both ends of the sample using a conductive silver paste.

3 Results and discussions

3.1 Structural analysis

Figure 3 depicts the XRD pattern of the as-deposited and the annealed layers. From this graph, both of the thin films deposited at 250 °C and annealed at 450 °C present an amorphous character. Whereas, the thin films annealed at 500 °C show an improvement crystallinity. Indeed, the characteristic peaks at 28.59°, 47.97° and 56.39° corresponding

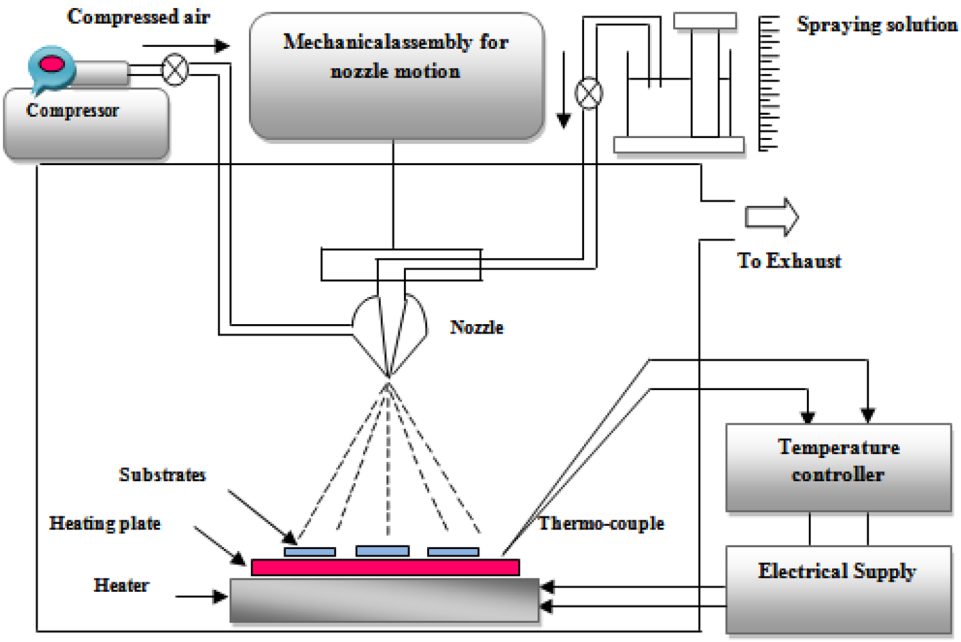

Fig. 1 Schematic of spray pyrolysis technique and its equipment

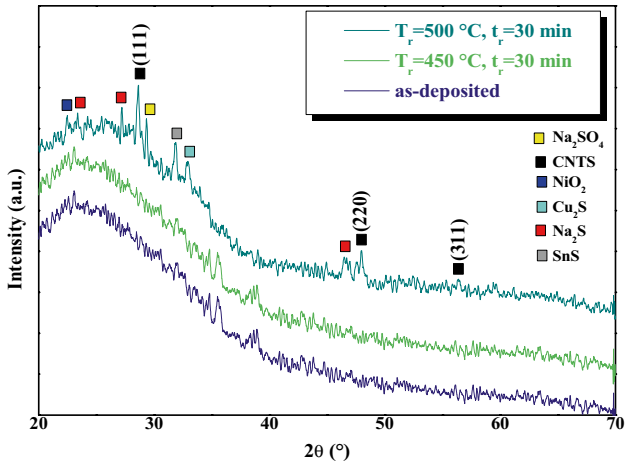

Fig. 3 X-ray spectra of the as-deposited and the annealed thin films

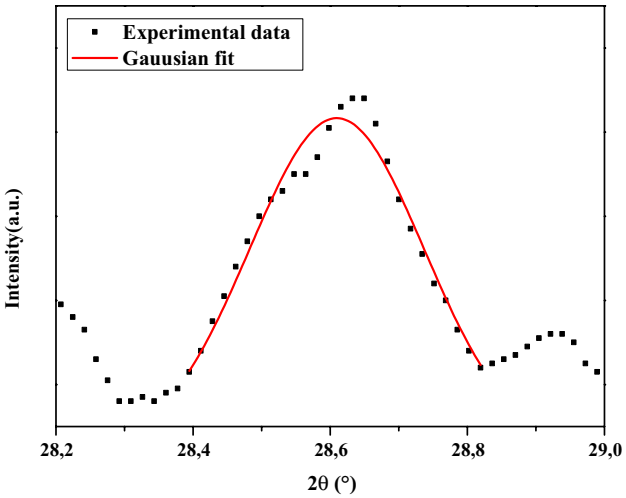

Fig. 4 The detailed measurement of (111) peak

to the (111), (220) and (311) planes related to the CNTS phase, respectively. Apart from these peaks, there were additional peaks including impurity phases such as binary compounds (NiO_2, Cu_2S, Na_2S, and SnS) and ternary compound (Na_2SO_4). Besides, the CNTS thin films exhibit a cubic structure in the space group F-43m. The above results coincide with the values reported by the Joint Committee on Powder Diffraction Standards (JCPDS) card number 00-026-0552 and also agree with the previous works reported by other authors [1, 6, 13].

The structural parameters such as reticular distance (d_{hkl}), lattice parameters (a, b and c), full width at half maximum (β), the average crystallite size (D), microstrain (ε) and dislocation density (δ) were determined. Using (111), (220) and (311) planes of CNTS thin films, the reticular distance d_{hkl} values, were calculated according to the Bragg equation [14]:

$$n\lambda = 2d_{hkl}\sin\theta, \tag{1}$$

As mentioned above, the CNTS thin films represent a cubic structure which leads to ($a=b=c$). Therefore, the lattice parameters were determined using the reticular distance formula:

$$d_{hkl} = \frac{a}{\sqrt{(h^2+k^2+l^2)}}. \tag{2}$$

The Gaussian fit of the main peak (111) is shown in Fig. 4. The average crystallite size (D) is calculated using the Debye–Scherrer formula [15]:

$$D = \frac{k\lambda}{\beta\cos\theta}, \tag{3}$$

where k is the shape factor ($k=0.9$), λ is the X-ray wavelength (1.5406 Å), β is the full width at half maximum (FWHM) and θ is the Bragg diffraction angle.

The microstrain (ε) can be expressed as follows [16]:

$$\varepsilon = \frac{\beta}{4\tan(\theta)}. \tag{4}$$

The dislocation density (δ) can be evaluated by Williamson and Smallman's formula [17]:

$$\delta = \frac{1}{D^2}. \tag{5}$$

Then, the detailed data, including the main structural parameters are listed in Table 1.

3.2 Morphological analysis

The surface image of the CNTS thin films was determined by scanning electron microscopy (SEM), as shown in Fig. 5a The surface of CNTS thin films is found to be uniform, rough and compact. No voids are observed throughout the whole glass substrate. As also seen, the SEM image demonstrates that several grains are agglomerated to each other. From the cross-sectional micrograph (Fig. 5b), the average-thickness is measured to be 1.36 µm (±0.05). This value is close to the thickness of CNTS material established by Kamble et al. [18].

3.3 Optical analysis

The optical absorption coefficient (α) is evaluated from the transmittance (T) and reflectance (R) measurements using the following relation [19]:

Table 1 Structural parameters of CNTS thin films

2θ (°)	(hkl)	d_{hkl}	$a=b=c$ (Å)	β (°)	D (nm)	ε (10^{-1})	δ (10^{-3} nm^{-2})
28.59	(111)	3.11	5.4	0.299	27.51	2.93	1.32
47.97	(220)	1.89	5.36	–	–	–	–
56.39	(311)	1.63	5.4	–	–	–	–

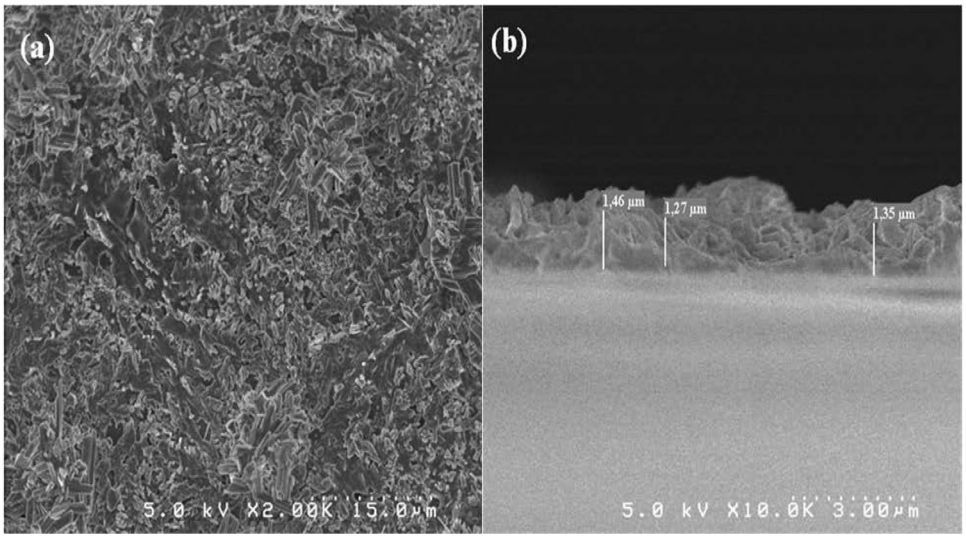

Fig. 5 **a** SEM micrograph of top surface and **b** cross section of CNTS thin films

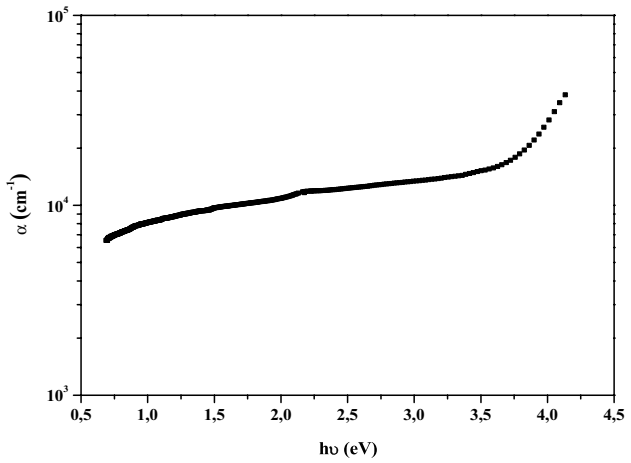

Fig. 6 Variation of absorption coefficient (α) versus photon energy ($h\nu$) of CNTS thin films

$$\alpha = \left(\frac{1}{d}\right) * \ln\left(\frac{(1-R)^2}{T}\right), \tag{6}$$

where d is the thickness. The variation of the absorption coefficient (α) with respect to photon energy ($h\nu$) for CNTS thin films is displayed in Fig. 6. It is observed that the absorption coefficient (α) increases slightly as the photon energy increases from 0.68 to 3.85 eV and afterwards continues to increase rapidly with the photon energy. Thereby, the evaluated value of (α) for CNTS thin films exceeds considerably 10^4 cm^{-1} in the visible region, indicating its use as an absorber layer in the solar cells.

On the other hand, the optical band gap energy (E_g) is obtained according to the Tauc's relation [20]:

$$(\alpha h\nu) = A(h\nu - E_g)^n, \tag{7}$$

where A is proportionality constant, h is Planck's constant, ν is the frequency of the incident photon and n equal to 1/2 or 2 for the direct and indirect band gap semiconductors, respectively. In our case $n=1/2$, the optical band gap is determined by extrapolating the tangent line of the curve $(\alpha h\nu)^2$ to the photon energies axis ($h\nu$). Figure 7 shows two linear portions which lead to two band gap values. And related to the XRD analysis, the band gap of 1.62 eV attributes to the CNTS phase and the second band gap of 2.06 eV can be correspond to Na_2S phase (~2 eV) or to Cu_2S phase (~2.37 eV) present in film [21, 22]. To conclude, the CNTS band gap energy of 1.62 eV is near with the optimal values for solar cell applications reported by other authors [4, 13, 23].

3.4 Electrical analysis

The complex impedance diagrams (Z' versus Z'') of CNTS thin films at different temperatures of 713–773 °K, were shown in Fig. 8. On the one hand, the single semicircular arcs, observed in complex impedance diagrams, are slightly

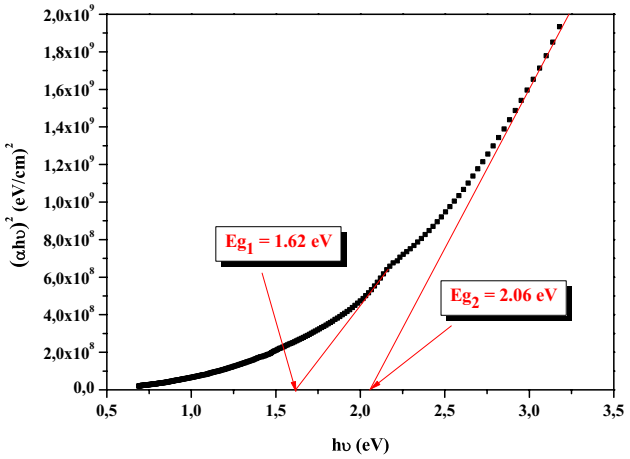

Fig. 7 Plot of $(\alpha h\nu)^2$ versus photon energy $(h\nu)$ of CNTS thin films

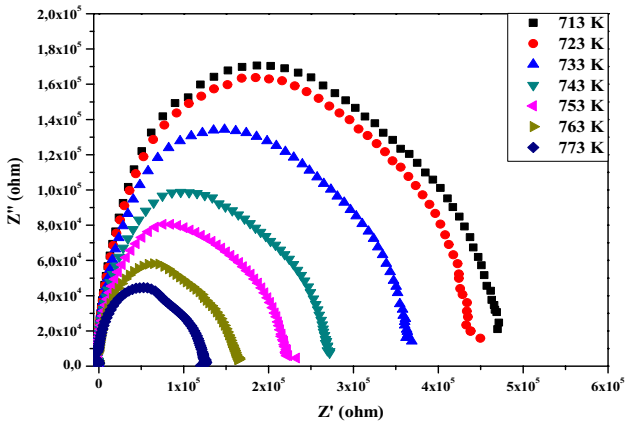

Fig. 8 Complex impedance diagrams (Z' versus Z'') of CNTS thin films at different temperatures

depressed and their centers shift towards higher frequency with the rise of temperature. The obtained of each semicircular arc presents the response of the grain contribution in materials. Figure 8 also interprets that each semicircular arc is an indicative of an electrical equivalent circuit, which comprises a capacitive element C placed in parallel with a resistive element R. On the other hand, the size of all semicircular arcs shrinks with the increase in temperature referring to pronounced reduce in the electrical resistivity [24]. As a result, these features correspond to a semiconductor behavior. Furthermore, the electrical conductivity and relaxation times are thermally activated. Similar results have also been reported by Bitri et al. for Cu_2ZnSnS_4 thin films [25].

As shown in Fig. 8, the resistance «R» values are ascertained from the intercept of semicircular arcs to the real axis and the associated capacitance «C» values are determined using the relation (8). Therefore, the main electrical parameters are collected in Table 2. From this table, the

Table 2 Electrical parameters of CNTS thin films

T (°K)	$\ln(\omega_m)$	ω_m (10^5)	R (10^5 Ω)
713	12.742	3.418	4.698
723	12.770	3.515	4.482
733	13.023	4.527	3.692
743	13.445	6.903	2.721
753	13.614	8.174	2.327
763	13.839	10.237	1.652
773	14.187	14.498	1.257

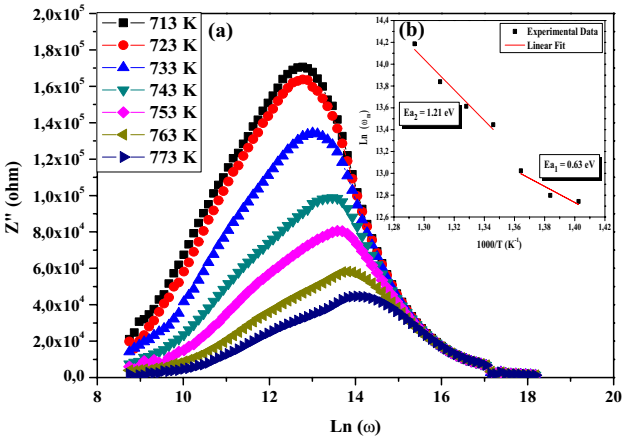

Fig. 9 **a** Plot of Z'' versus $\ln(\omega)$, and **b** $\ln(\omega_m)$ versus $(1000/T)$ of CNTS thin films

resistance «R» value decreases with increasing temperature. While the frequency ω_m value increases with the temperature.

The spectra in Fig. 9 give the variation of the imaginary part of impedance Z'' with the frequency of CNTS thin films. The magnitude of imaginary impedance Z'' increases initially up to reach a maximum peak and afterwards begin to decrease with frequency. In the same line, the maximum in Z'' peak merges in the higher frequency region with the increase in temperature. Besides, the frequency ω_m matching at Z'' maximum is given by the reciprocal of the relaxation time τ:

$$\omega_m = \frac{1}{\tau} = \frac{1}{RC}. \tag{8}$$

The temperature dependence of angular frequency ω_m is found to follow the Arrhenius equation [26]:

$$\omega_m = \omega_0 e^{\frac{-E_a}{k_B T}}, \tag{9}$$

where ω_0 is constant, E_a is the activation energy, and k_B is the Boltzmann constant. As shown in Fig. 9b (inset graph),

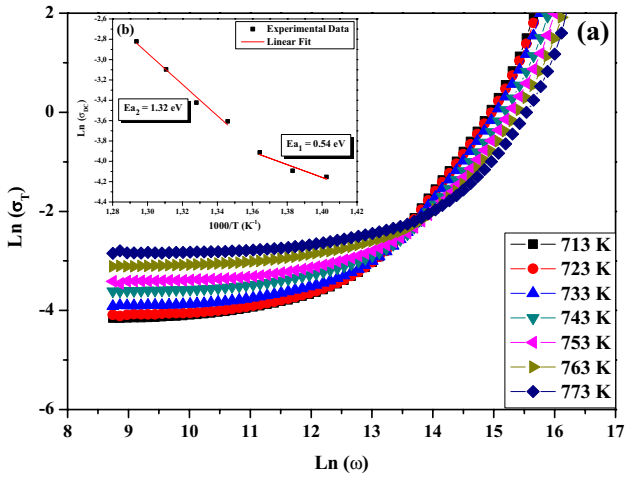

Fig. 10 **a** Plot of $\ln(\sigma_T)$ versus $\ln(\omega)$, and **b** $\ln(\sigma_{DC})$ versus $(1000/T)$ of CNTS thin films

the slope of the linear fit obtained from the plot of $\ln(\omega_m)$ versus $(1000/T)$ leads to the activation energy.

The CNTS thin films present two activation energies $E_{a1} = 0.63$ eV and $E_{a2} = 1.21$ eV. The presence of second activation energy can be attributed to the formation of secondary phases in film.

Figure 10 presents the variation of total conductivity σ_T in the low- and high-frequency regions (I and II) of CNTS thin films at different temperatures. Region I demonstrates that the total conductivity is almost unchanged with frequency, which can be attributed to DC contribution. While, region II proves that the total conductivity increases linearly with frequency, which corresponds to the AC conductivity. A distinct change in the slope of total conductivity from frequency independent (region I) to frequency dependent (region II) suggests the phenomenon of conductivity relaxation [27, 28]. Subsequently, the total conductivity «σ_T» is given by:

$$\sigma_t = \sigma_{DC} + \sigma_{AC}, \tag{10}$$

where «σ_{DC}» is the DC conductivity obtained by extrapolation of the curves of «σ_T» to zero frequency at different temperatures and «σ_{AC}» is the AC conductivity as well defined via Jonscher's universal power law:

$$\sigma_{AC}(\omega) = A\omega^S. \tag{11}$$

Here A is a complex proportionality constant and «s» is an exponent, which has a value less than or equal to the unity.

The temperature dependence of DC conductivity is found to follow the Arrhenius equation [26]:

$$\sigma_{DC} = \sigma_0 e^{\frac{-E_a}{k_B T}}, \tag{12}$$

where σ_0 is constant.

As illustrated in Fig. 10b (inset graph), the activation energy is determined from the slope of the $\ln(\sigma_{DC})$ versus $(1000/T)$. The activation energies $E_{a1} = 0.54$ eV and $E_{a2} = 1.32$ eV are consistent with those deduced from angular frequency. The values obtained from the angular frequency and DC conductivity indicate that the carrier transport mechanism is thermally activated in the band gap. These results are in agreement with our DRX and optical results.

4 Conclusions

In summary, CNTS thin films were successfully prepared, for the first time, by the «Spray pyrolysis» technique followed by an annealing treatment process. XRD studies reveal that the CNTS thin films present a cubic structure with preferential orientation along (111) direction. SEM micrograph reveals that the surface of CNTS thin film uniform, rough and compact. UV/Vis absorption spectra indicate that CNTS thin films have a high optical absorption (10^4 cm^{-1}) in the visible region and the direct band energy of 1.62 eV. Impedance spectroscopy studies show single semicircular arcs, which can be described by an electrical equivalent *R–C* circuit. Thereby, it is shown in complex impedance diagrams that the resistance *R* decreases with increasing temperature, which corresponds to a semiconductor behavior. In the end, the activation energy value esteemed from angular frequency is identical to this calculated from DC conductivity, indicating that the carrier transport mechanism is thermally activated in the band gap. These results open the possibility to use the CNTS material as an active layer in thin film solar cells.

Acknowledgements The authors would like to acknowledge Tunisian Ministry of Higher Education and Scientific Research for financial support of this work and to thank Mrs Isabelle Ly for her help with the MEB characterizations measurements from CRPP (University Bordeaux 1).

References

1. S. Sarkar, B. Das, P.R. Midya, G.C. Das, K.K. Chattopadhyay, Optical and thermoelectric properties of chalcogenide based Cu_2NiSnS_4 nanoparticles synthesized by a novel hydrothermal route. Mater. Lett. **152**, 155–158 (2015)
2. A. Kamble, K. Mokurala, A. Gupta, S. Mallick, P. Bhargava, Synthesis of Cu_2NiSnS_4 nanoparticles by hot injection method for photovoltaic applications. Mater. Lett. **137**, 440–443 (2014)
3. H.-J. Chen, S.-W. Fu, T.-C. Tsai, C.-F. Shih, Quaternary Cu_2NiSnS_4 thin films as a solar material prepared through electrodeposition. Mater. Lett. **166**, 215–218 (2016)
4. C.L. Yang, Y.H. Chen, M. Lin, S.L. Wu, L. Li, W.C. Liu, X.S. Wu, F.M. Zhang, Structural, optical and magnetic properties of Cu_2NiSnS_4 thin films deposited by facile one-step electrodeposition. Mater. Lett. **166**, 101–104 (2016)
5. Y. Cui, R. Deng, G. Wang, D. Pan, A general strategy for synthesis of quaternary semiconductor Cu_2MSnS_4 ($M = Co^{2+}$, Fe^{2+}, Ni^{2+}, Mn^{2+}) nanocrystals. J. Mater. Chem. **22**, 23136 (2012)
6. T.-X. Wang, Y.-G. Li, H.-R. Liu, H. Li, S.-X. Chen, Flower-like Cu_2NiSnS_4 nanoparticles synthesized by a facile solvothermal method. Mater. Lett. **124**, 148–150 (2014)
7. L. Shi, Y. Li, R. Zheng, Nanoconfined solvothermal synthesis and characterization of ultrafine Cu_2NiSnS_4 nanotubes. ChemPlusChem **80**, 1533–1536 (2015)
8. F. Ozel, Earth-abundant quaternary semiconductor Cu2MSnS4 (M=Fe Co, Ni and Mn) nanofibers: fabrication, characterization and band gap arrangement. J. Alloys Compd. **657**, 157–162 (2016)
9. A. Ghosh, A. Biswas, R. Thangavel, G. Udayabhanu, Photo-electrochemical property and electronic band structure of kesterite copper chalcogenides Cu_2-II-Sn-S_4 (II = Fe Co, Ni) thin films. RSC Adv. **6**, 96025–96034 (2016)
10. S. Dridi, N. Bitri, M. Abaab, Synthesis of quaternary Cu_2NiSnS_4 thin films as a solar energy material prepared through «Spray» technique. Mater. Lett. **204**, 61–64 (2017)
11. N. Bitri, S. Dridi, F. Chaabouni, M. Abaab, Studies on the electrical properties of Cu_2NiSnS_4 thin films prepared by a simple chemical method. Mater. Lett. **213**, 31–34 (2018)
12. D. Perednis, L.-J. Gauckler, Thin film deposition using spray pyrolysis. J. Electroceram. **14**, 103–111 (2005)
13. A. Jariwala, T.K. Chaudhuri, S. Patel, A. Toshniwal, V. Kheraj, A. Ray, Direct-coated copper nickel tin sulphide (Cu_2NiSnS_4) thin films from molecular ink. Mater. Lett. **215**, 118–120 (2018)
14. J. Kacher, C. Landon, B.L. Adams, D. Fullwood, Bragg's Law diffraction simulations for electron backscatter diffraction analysis. Ultramicroscopy **109**, 1148–1156 (2009)
15. C. Barret, T.B. Massalki, *Structure of Metals* (Oxford Pergamon, Oxford, 1980)
16. A. Jebali, N. Khemiri, M. Kanzari, The effect of annealing in N_2 atmosphere on the physical properties of $SnSb_4S_7$ thin films. J. Alloys Compd. **673**, 38–46 (2016)
17. G.K. Williamson, R.E. Smallman, Dislocation densities in some annealed and cold worked metals from measurements on the X-ray Debye-Scherrer spectrum. Philos. Mag. **1**, 34–45 (1956)
18. A. Kamble, K. Mokurala, P. Bhargava, S. Mallick, Solution Processed Cu_2NiSnS_4 Nanoparticles: Potential Absorber Material For Thin Film Solar Cells, *42nd Photovoltaic Specialist Conference (PVSC)* (2015)
19. M. Caglar, S. Ilican, Y. Caglar, Influence of dopant concentration on the optical properties of ZnO: In films by sol–gel method. Thin Solid Films **517**, 5023–5028 (2009)
20. E.A. Davis, N.F. Mott, Conduction in non-crystalline systems V Conductivity, optical absorption and photoconductivity in amorphous semiconductors. Philos. Mag. **22**, 0903–0922 (1970)
21. P. Pandit, B. Rakshit, S.P. Sanyal, Electronic and elastic properties of alkali-metal sulphides-Li_2S and Na_2S. Indian J. Pure Appl. Phys. **47**, 804–807 (2009)
22. N.K. Allouche, T.B. Nasr, C. Guasch, N.K. Turki, Optimization of the synthesis and characterizations of chemical bath deposited Cu_2S thin films. C. R. Chimie **13**, 1364–1369 (2010)
23. S. Rondiya, N. Wadnerkar, Y. Jadhav, S. Jadkar, S. Haram, M. Kabir, Structural, electronic, and optical properties of Cu_2NiSnS_4: a combined experimental and theoretical study toward photovoltaic applications. Chem. Mater. **29**, 3133–3142 (2017)
24. I.B. Jemaa, F. Chaabouni, M. Abaab, Investigation into the opto-electrical properties of TiO_2 thin films, deposited by RF magnetron sputtering using powder target. Phys. Status Solidi A **214**, 1600426 (2017)
25. N. Bitri, S. Mahjoubi, M. Abaab, I. Ly, Electrical properties of Cu_2ZnSnS_4 thin films deposited by spray-sandwich technique. Mater. Lett. **219**, 194–197 (2018)
26. C.R. Mariappan, G. Govindaraj, S.V. Rathan, G.V. Prakash, Vitrification of $K_3M_2P_3O_{12}$ (M = B, Al, Bi) NASICON-type materials and electrical relaxation studies. Mater. Sci. Eng. B **123**, 63–68 (2005)
27. A.A. Ali, M.H. Shaaban, Electrical properties of LiBBaTe glass doped with Nd_2O_3. Solid State Sci. **12**, 2148–2154 (2010)
28. R.V. Bardea, K.R. Nemade, S.A. Waghuley, AC conductivity and dielectric relaxation in V_2O_5–P_2O_5–B_2O_3 glasses. J. Asian Ceram. Soc. **3**, 116–122 (2015)